Proceedings of the 7th International Symposium on Cavitation
CAV2009 – Paper No. 33
August 17-22, 2009, Ann Arbor, Michigan, USA

Prediction of cavitation erosion based on the measurement of bubble collapse impact loads

Shuji Hattori
Graduate School of Engineering,
University of Fukui
Fukui-shi, Fukui, Japan

Takuya Hirose
Graduate School of Engineering,
University of Fukui
Fukui-shi, Fukui, Japan

Kenichi Sugiyama
Ebara Corporation
Fujisawa-shi, Kanagawa, Japan

ABSTRACT

The prediction of cavitation erosion rates is important in order to evaluate the exact life of components in fluid machineries. The measurement of impact loads in bubble collapses helps us to predict the life under cavitation erosion. In this study, we carried out the erosion tests and measured impact loads in bubble collapses with a cavitating liquid jet apparatus which complies with the ASTM G134-95 standard. The bubble collapse impact loads were measured by a piezo ceramic transducer in a cavitating liquid jet apparatus. To produce various cavitation conditions, the flow velocity was changed from 184 down to 80 m/s. We evaluated the incubation period based on a cumulative damage rule by measuring the impact loads of cavitation acting on the specimen surface and by using the "constant impact load – number of impact curve" similar to the modified Miner's rule which is employed for fatigue life prediction. We found that the parameter $\sum(F_i^{\alpha}\times n_i)$ (F_i: impact load, n_i: number of impacts and α: constant) is suitable for the evaluation of the erosion life. After the constant α has been obtained under two different cavitation conditions, we can predict the incubation period with the cavitating liquid jet method under yet another condition, provided that the bubble collapse impact loads are measured.

INTRODUCTION

Cavitation often occurs in the contact area between solids and liquids in fluid machineries, pipes, ship propellers, valves and so on. The erosion is a phenomenon that erodes the component surface sponge-like. Cavitation erosion is a serious problem that brings a performance reduction of an apparatus or a life reduction by component failure. The measurement of impact loads in bubble collapses (bubble collapse impact loads) helps us to predict the cavitation erosion.

Hattori et al. [1] measured bubble collapse impact loads using a venturi test facility and a vibratory apparatus, and clarified the relation between the cumulative impact energy $\sum F_i^2$ (F_i: impact load from an individual bubble collapse) obtained from the impact load distribution and the erosion volume loss rate. For low $\sum F_i^2$ (near the cavitation damage threshold), however, the relation between $\sum F_i^2$ and the volume loss has not yet been clarified. On the other hand, Iwai et al. [2] reported a good proportional relation between the fatigue damage $\sum(n_i/N_i)$ (N_i: number of cycles to failure) calculated at stress amplitudes above a certain threshold value and the incubation period by using a vibratory apparatus, and between $\sum(n_i/N_i)$ and the volume loss rate in the steady period. However, there is an issue that a basic S-N curve against the erosion rate has to be assumed [2] and the threshold value of the impact loads without the influence of erosion has to be found experimentally. Soyama et al. [3] carried out a cavitation test using a sheet of pure aluminum glued to a pump impeller, and obtained the bubble collapse impact loads from the deformation of the aluminum sheet. They proposed a threshold for the erosion energy below which erosion does not occur. However, the physical meaning of the erosion energy threshold was not clarified. In [4] we carried out the erosion tests and measured the bubble collapse impact loads under the different cavitation intensities with a vibratory apparatus, and proposed a prediction method for the incubation period. However, the applicability of the prediction method to a flowing system was not clarified.

In this study, we have carried out erosion tests and measured the bubble collapse impact loads by a piezo ceramic transducer (sensor) using a cavitating liquid jet which can provide an erosion test under conditions similar to a prototype machine. We discuss a prediction method for the incubation period under various cavitation conditions.

TEST MATERIALS AND METHOD

The test materials are pure aluminum to determine the optimum stand-off distance according to ASTM G134-95 [5], S15C low carbon steel (0.15 % carbon steel), SUS304 austenite stainless steel with high corrosion resistance and STPA24 alloy steel for pipes. The chemical composition and the physical and mechanical properties of these materials are listed Tables 1 and 2, respectively. The shape of each test specimen is 12 mm in diameter and 4 mm in thickness, as shown in Figure 1. The test specimen surface was mirror-finished by buffing after being polished with emery paper up to grade #1200.

Figure 2 shows the cavitating liquid jet test chamber which is specified in the ASTM G134-95 standard [5]. The test liquid

Table 1: Chemical composition of test materials

(mass%)

Material	C	Si	Mn	V	P	S	Cu	Ni	Mo	Cr	Al	Fe	Ti
Al	-	0.06	-	0.01	-	-	0.01	-	-	-	Bal	0.12	0.01
S15C	0.16	0.21	0.45	-	0.01	0.016	0.01	0.02	-	0.05	-	Bal	-
SUS304	0.06	0.2	1.67	-	0.034	0.027	-	8.0	-	18.73	-	Bal	-
STPA24	0.12	0.35	0.47	0.002	0.012	0.004	0.02	0.02	0.93	2.12	0.002	Bal	0.001

Table 2: Physical and mechanical properties of test materials

Material	Density kg/m^3	Tenile strength MPa	Vickers hardness $HV_{0.2}$
Al	2.71×10^3	95	38
S15C	7.81×10^3	441	145
SUS304	7.93×10^3	792	171
STPA24	7.72×10^3	630	216

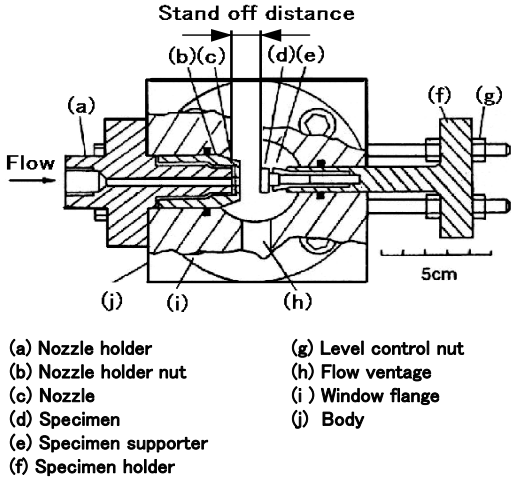

Figure 2: Test chamber

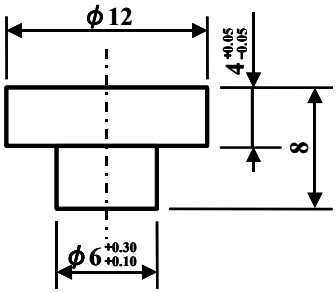

Figure 1: Shape of test specimen

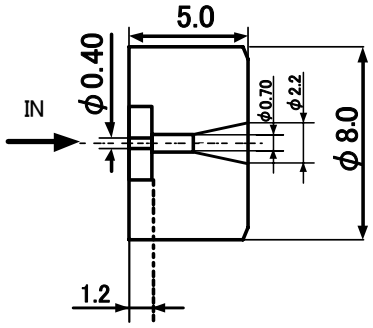

Figure 3: Nozzle shape

was tap water kept at 35±2 degrees C. The cavitation erosion tests were carried out in a test chamber. Figure 3 shows the nozzle shape used for the test. The nozzle shape is different from that specified in the ASTM standard, but it is clarified that erosion test results by the cavitating jet method are equal in spite of the difference of the nozzle shape [6]. Therefore, we carried out erosion tests by using the nozzle as shown in Figure 3. To produce various cavitation conditions, the flow velocity was changed by controlling upstream and downstream pressures (both were absolute pressures) at a constant cavitation number of 0.025. The flow velocity V is given by the following equation,

$$V = \sqrt{\frac{2(p_u - p_d)}{\rho}} \tag{1}$$

where ρ is the liquid density, p_u is the upstream pressure (absolute pressure MPa) and p_d is the downstream pressure (absolute pressure MPa). The cavitation number σ shows the tendency for cavitation to occur in flowing streams of liquids, and is defined by the following equation,

$$\sigma = \frac{p_d - p_v}{p_u - p_d} \tag{2}$$

where p_v is the vapor pressure (absolute pressure MPa). The test specimen was removed periodically at predetermined time intervals, and weighed with a precision balance (sensitivity of 0.01 mg) after cleaning with acetone in an ultrasonic bath. The test result was expressed by using the MDE (Mean Depth of Erosion), i.e. the mass loss divided by the density of material and the eroded area.

In the cavitation erosion tests, the amount of erosion reaches a maximum at the location where most bubbles collapse. Therefore, a preliminary test was carried out to determine the optimum stand-off distance. Figure 4 shows the relation between the stand-off distance (the distance between the inlet edge of the nozzle and the target face of the specimen) and the mass loss of the pure aluminum specimen after a test for 30 minutes. Since the amount of erosion reached the maximum at a stand-off distance of 10 mm, the optimum stand-off distance was determined to be 10 mm.

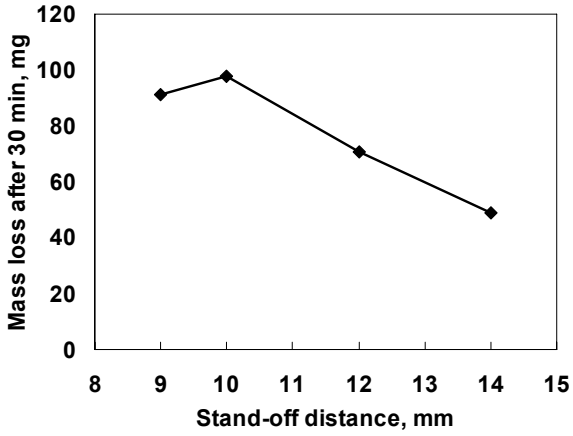

Figure 4: Relation between stand-off distance and mass loss of Al

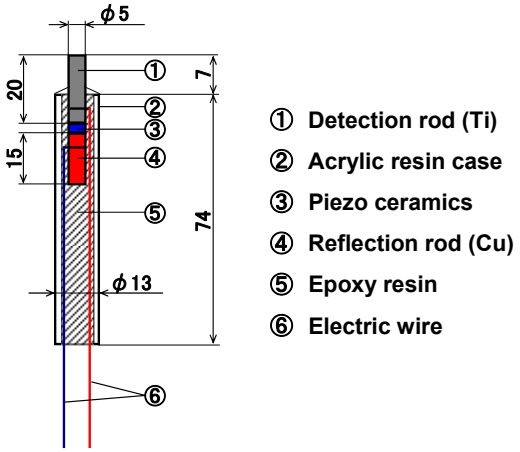

Figure 5: Sensor structure

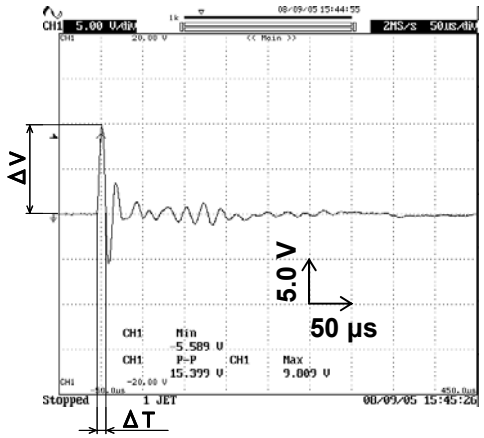

Figure 6: An example of output waveform by a steel ball drop test from a height of 100 mm

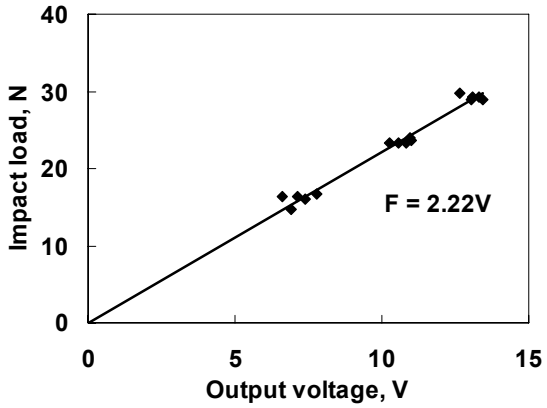

Figure 7: Relation between output voltage and impact load

The bubble collapse impact loads were measured under the same conditions as in the cavitation erosion test by using a piezo ceramic transducer (sensor) instead of the test specimen. The bubble collapse impact loads were measured for 1 minute. Figure 5 shows an illustration of the sensor structure. The piezo ceramic for detecting impact loads is a disk of 5 mm in diameter and 0.2 mm in thickness. The piezo ceramic was sandwiched between the 5 mm detection rod made of Ti and the reflection rod of Cu, and fixed with a conductive adhesive. An epoxy resin agent was used to fill in the space between the part of the pressure detector and the acrylic resin pipe for making it vibration-proof, water-proof and for protection from breakage of the ceramic disk. The sensor performance depends on the surface profiles of the detection rod and the reflection rod and on the adhesive condition of the piezo ceramic. To eliminate the differences in sensor performance, we carried out a steel ball drop test to obtain a calibration coefficient for the sensor before the measurement of bubble collapse impact loads. In the steel ball drop test, a steel ball (0.134g) made of SUS304 was dropped on the detection surface of the sensor, and the output waveform in Figure 6 was read using an oscilloscope. The maximum voltage ΔV [V] and the hold time of the impact load ΔT [μs] were obtained. The impact load detected at the sensor F can be obtained from following equation by the energy conservation law and the impulse.

$$F = m \times (1 + e_1) \times \frac{V_0}{\Delta T} = 5.94 \times 10^{-4} \times (1 + e_1) \times \frac{\sqrt{h_0}}{\Delta T} \quad (3)$$

where m is mass of the steel ball (=0.134×10^{-3} kg), e_1 is rebound restitution coefficient of Ti (=0.71), V_0 is impact velocity (=$\sqrt{2gh_0}$), g is acceleration of gravity, ΔT is hold time of the impact load and h_0 is drop height. The appropriate calibration coefficient of the sensor was obtained from the relation between the voltage and the impact load. The relation between the voltage ΔV and the impact load F of the sensor used in this study was F=2.22ΔV as shown in Figure 7.

Figure 8 shows the diagram for the measurement of the bubble collapse impact loads. The output signal obtained from the sensor was passed through the high-pass filter to cut the low frequencies, and then fed into the computer with A/D conversion after being processed in the peak-hold circuit. A real output pulse of the cavitation after it passed through the circuit

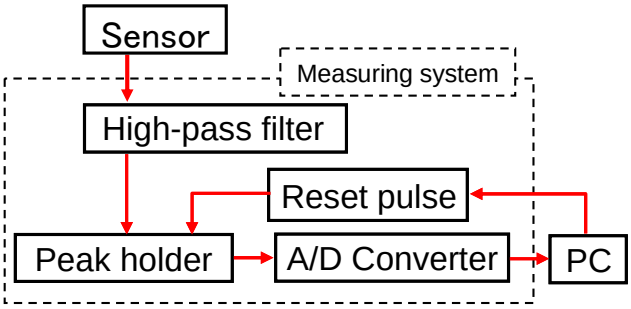

Figure 8: Diagram for measurement of bubble collapse impact loads

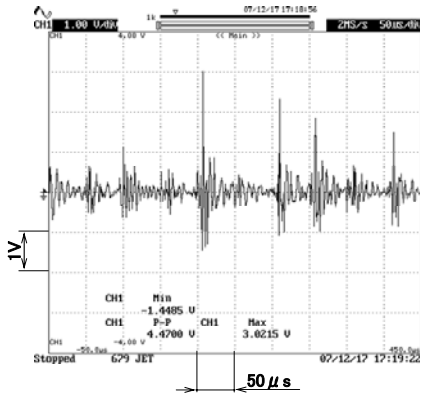

Figure 9: An example of output pulse by cavitation

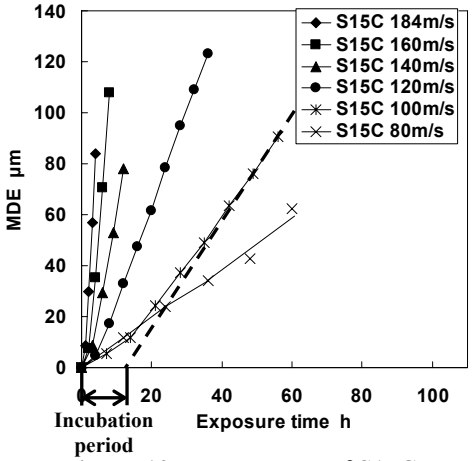

Figure 10: MDE curves of S15C

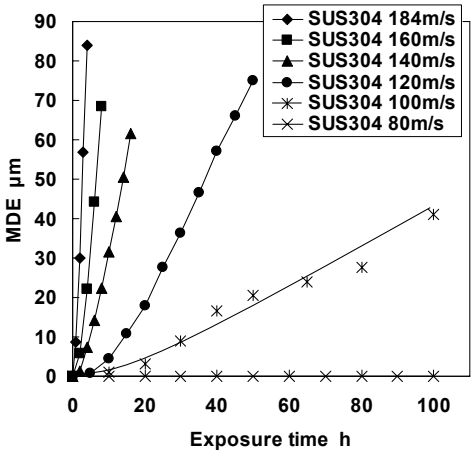

Figure 11: MDE curves of SUS304

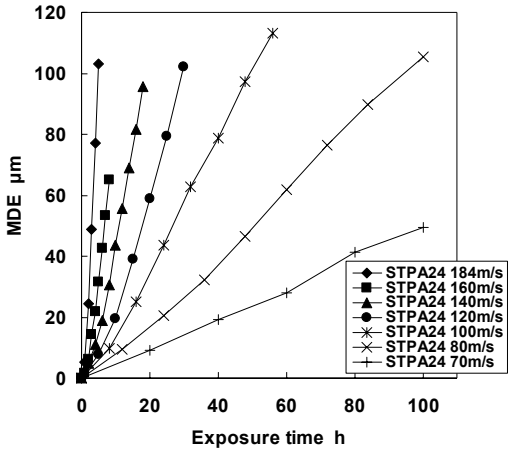

Figure 12: MDE curves of STPA24

Table 3: Incubation period of test materials

Material	Incubation period [min]					
	Flow velocity					
	184m/s	160m/s	140m/s	120m/s	100m/s	80m/s
S15C	54	120	144	216	450	1320
SUS304	54	126	210	636	852	
STPA24	72	132	216	348	384	612

is shown in Figure 9. It is thought that the bubble collapse impact load acts at the high output voltage in Figure 9. However, the hold time of bubble collapse impact loads is as short as about 1.5 μs. Therefore, the peak-hold circuit was used. To consider the influence of the voltage reduction in the circuit, we determined the calibration coefficient of the circuit from the relation between the input voltage and the output voltage of an artificial pulse wave of frequency 1 kHz and with the height of the pulse wave being adjusted to between 0 and 5.0 V. The pulse wave was generated using a function generator and the output voltage was obtained from of the height of the pulse wave on an oscilloscope after it passed through the circuit. The relation between the input voltage V_{in} and the output voltage V_{out} of the measuring system used in this study was V_{in}=2.618V_{out}. Therefore, we were able to obtain bubble collapse impact loads and their counts using calibration factor of the sensor and the circuit.

TEST RESULTS AND DISCUSSION

Figure 10 shows the MDE (Mean depth of erosion) curves of S15C at flow velocities from 184 down to 80 m/s, Figure 11 shows the MDE curves of SUS304 and Figure 12 shows the curves of STPA24. All MDE curves pass through an incubation period with low erosion rate and then they increase to reach a maximum rate period for each material. When the materials are compared at the same exposure time, the MDE of SUS304 is lower than that of S15C since SUS304 is harder than S15C. This corresponds to our previous finding [7] that the erosion rate has a good correlation with the hardness. However, when SUS304 is compared with the harder STPA24, the MDE of STPA24 is higher. This is because the work hardening of the stainless steel of SUS304 is higher than that of the STPA24.

Table 3 shows the incubation period for each material. The periods were obtained from Figures 10, 11 and 12 as the point

of intersection of the extended straight line of the slope of the maximum rate period with the axis of the exposure time. The incubation period of S15C with lower hardness is shorter than that of SUS304 with higher hardness. This is because cracks initiate easily for low hardness materials, because plastic deformation can occur even at low impact loads, when the various impact loads act on the material surface.

Figure 13 shows the distribution of the bubble collapse impact loads, measured with the sensor located at the optimum stand-off distance of 10 mm. Several thousand to several tens of thousands of counts/minute of small impact loads were detected, while lower numbers of counts/minute at large impact loads were measured. The distributions at various flow velocities are very similar, and the frequency of the large impact loads is higher at higher flow velocities.

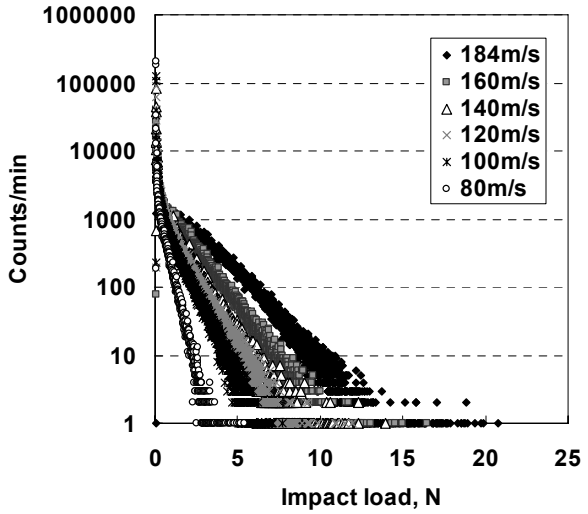

Figure 13: Distribution of bubble collapse impact loads

When the impact load F_i acts on the specimen surface during the holding time ΔT, the impact energy e is given [8], [9] by

$$e = \Delta T / \rho c \times F_i^2 \tag{4}$$

where ρ is the density of the test liquid and c is the sound velocity in the liquid. If the holding time ΔT is assumed to be constant irrespective of the magnitude of the impact load acting on the specimen, the cumulative impact energy E for various impact loads F_i on the specimen surface can be assumed to obey

$$E \propto \sum F_i^2 \tag{5}$$

This means the cumulative impact energy E is in proportion to the cumulative square value of impact loads ($\sum F_i^2$). $\sum F_i^2$ can be calculated with $\sum(F_i^2 \times n_i)$ using the impact load F_i and its counts n_i obtained from the measurement of the bubble collapse impact loads.

Figure 14 shows the relation between $\sum F_i^2$ and the maximum erosion rate $MDER_{max}$ at each flow velocity obtained in this study. $MDER_{max}$ is the maximum slope in the maximum rate period of the MDE curve. $MDER_{max}$ increases linearly with $\sum F_i^2$ for all materials. The linear relation between $\sum F_i^2$ and the erosion rate was reported [1]. Since we focus on the incubation period in the present study, the evaluation by $MDER_{max}$ is not suitable. Therefore, we here evaluated with the incubation period at each flow velocity. Figure 15 shows the relation between $\sum F_i^2$ and the reciprocal of the incubation period obtained in this study. Straight lines can be drawn passing through the origin, but the accuracy of this relation is not so good. Therefore, we discuss the prediction method from another viewpoint.

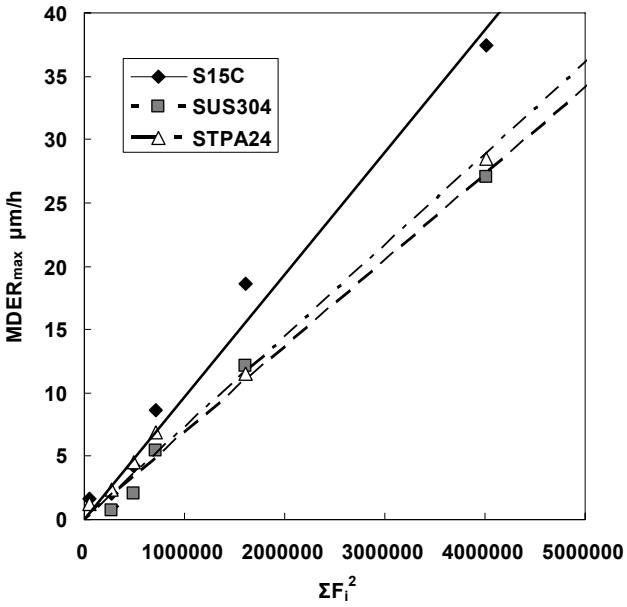

Figure 14: Relation between $\sum F_i^2$ and $MDER_{max}$

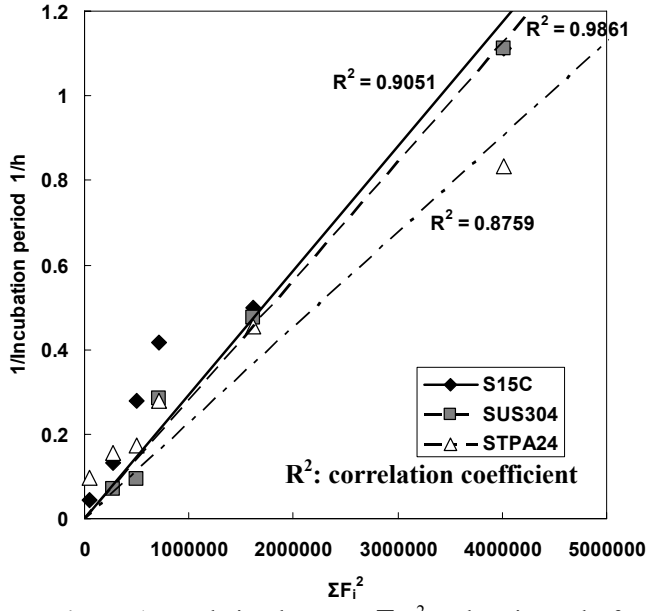

Figure 15: Relation between $\sum F_i^2$ and reciprocal of the incubation period

Hammitt et al. [10] reported that the erosion proceeds by fatigue failure. Vaidya and Preece [11] reported that fatigue striation was observed on the eroded surface of Al-4%Cu alloy. The damage mechanism of components subjected to cavitation bubble collapse impact loads is therefore regarded as fatigue failure under the variable amplitude stress. We therefore discuss cavitation erosion from the viewpoint of fatigue life.

The linear cumulative damage rule is one of the prediction methods for the fatigue life under variable amplitude loading. Figure 16 shows the schematic S-N curves on a double logarithmic scale [12]. The slope part is given by

$$\sigma_i^{\alpha} \times N_i = C \tag{6}$$

where σ_i is rotary bending stress and N_i is number of cycles of σ_i to fracture. Nakamura et al. [13] proposed that the S-N curve on a double logarithmic scale should be used to predict the fatigue life. The fatigue damage is given by the cycle ratio n_i/N_i when σ_i is repeated n_i times under variable amplitude stress. It is assumed that the damage at each stress level is independent and is accumulated linearly. It is further assumed that the material ruptures when the sum of the cycle ratios n_i/N_i reaches unity. This sum is given by

$$D = \sum \frac{n_i}{N_i} = 1 \tag{7}$$

where n_i is number of cycles of σ_i.

The solid line in Figure 16 shows the S-N curve in order to predict the fatigue life using Miner's rule, assuming that fatigue damage does not occur below the fatigue limit. The broken line in Figure 16 is based on the modified Miner's rule which assumes that all stresses contribute equally to the fatigue damage. The result was that fatigue damage is accumulated due to the stress even below the fatigue limit under variable amplitude stress, when the stress is combined with stresses above the fatigue limit [12]. The modified Miner's rule is nowadays commonly used [12] to evaluate fatigue damage.

Since many impact loads at various intensities are measured in cavitation bubble collapses, the modified Miner's rule under the variable amplitude loading is applied to the prediction of

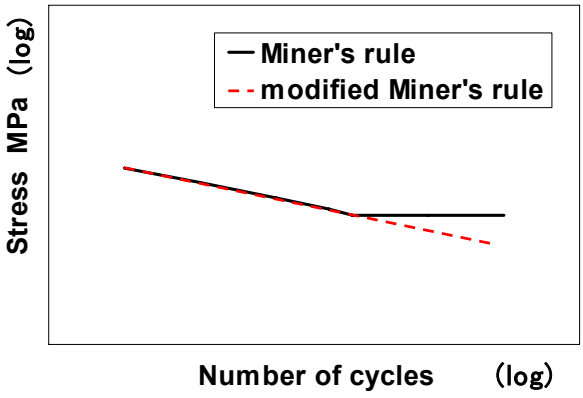

Figure 16: Schematic S-N curves

cavitation erosion. The incubation period is defined as the point of intersection of the extended straight line of slope of the maximum rate period with the axis of exposure time [5], and the termination of incubation period is well assumed to coincide with macroscopic fatigue failure. The incubation period has been discussed based on the accumulation of fatigue damage.

The prediction method of cavitation erosion was constructed on the basis of the modified Miner's rule by using the relation between the impact load F_i and the number of impacts per unit time n_i obtained from the measurement of bubble collapse impact loads at the various flow velocities. The incubation periods were obtained from the cavitation erosion test at the various flow velocities. Since it is impossible to measure the impacted area, we cannot convert the force to a stress. Therefore, the F-N curve was used. N is the impact number at the termination of the incubation period with constant impact load F. Since a test with a constant impact load F_i cannot be carried out for cavitation erosion, the impact number at the termination of incubation period N_i is basically unknown. But, the F-N curve is derived using constant parameters of α and C in

$$F_i^{\alpha} \times N_i = C \tag{8}$$

The parameter $\sum(n_i/N_i)$ is the cumulative damage per unit time. The incubation period t_d (the subscript d indicates the flow velocity) finishes when $\sum(n_i/N_i)$ becomes unity. t_d is therefore given as

$$t_d = \frac{1}{\sum \frac{n_i}{N_i}} \tag{9}$$

To determine the constants α and C, the unknown number N_i in Eq. (8) is expressed by F_i and the constants α and C, and then substituted into Eq. (9). This result shows the following equation.

$$\frac{1}{C}\sum\left(F_i^{\alpha} \times n_i\right) = \frac{1}{t_d} \tag{10}$$

For a given material, the constants α and C are independent of the impact load F_i, the number of impacts n_i and the incubation period t_d. Therefore Eq. (10) with the data at a flow velocity of 184 m/s was divided by Eq. (10) with the data at a flow velocity of 160 m/s, which gives the following relation.

$$\frac{\sum\left(F_{i,184}^{\alpha} \times n_{i,184}\right)}{\sum\left(F_{i,160}^{\alpha} \times n_{i,160}\right)} = \frac{t_{160}}{t_{184}} \tag{11}$$

Since t_d, F_i and n_i are already given, the constant α can now be determined with a trial & error method using Eq. (11). After α is determined, the constant C can be obtained from Eq. (10). Since the constants α and C are different depending on the

material, it is necessary to find them for each material. Table 4 shows the values of α and C for the various materials.

The parameter $\sum F_i^2$ has been used previously to evaluate the erosion [1]. We have already discussed the erosion using the parameter $\sum(F_i^{\alpha}\times n_i)$ in Eq. (10). Figure 17 shows the relation between the parameter $\sum(F_i^{\alpha}\times n_i)$ and the reciprocal of the incubation period obtained from the cavitation erosion tests of the various metals and flow velocities. Straight lines can be drawn passing through the origin. Furthermore, by comparing Figure 17 with Figure 15, the R^2 value increases for all materials and it is understood that the accuracy of $\sum(F_i^{\alpha}\times n_i)$ is better than that of $\sum F_i^2$. Therefore, the parameter $\sum(F_i^{\alpha}\times n_i)$ is suitable for the evaluation of cavitation erosion. By using the values of α and C obtained from two different cavitation conditions, we can predict the incubation period t_d by Eq. (10) using the values of F_i and n_i obtained from measurement of bubble collapse impact loads at each flow velocity. Figure 18 shows the relation between the predicted incubation periods and the measured incubation period for each flow velocity, plotted on a double logarithmic scale. A straight line with a slope of 45° on the double logarithmic scale was obtained. This shows that this prediction has a very high accuracy.

In this study, we clarified that the incubation period can be predicted if the constants α and C are obtained from erosion test and the measurement of bubble collapse impact loads under two different cavitation conditions.

Table 4: α and C of each material

Material	α	C
S15C	1.64	1.29E+08
SUS304	1.79	1.59E+08
STPA24	1.11	8.89E+07

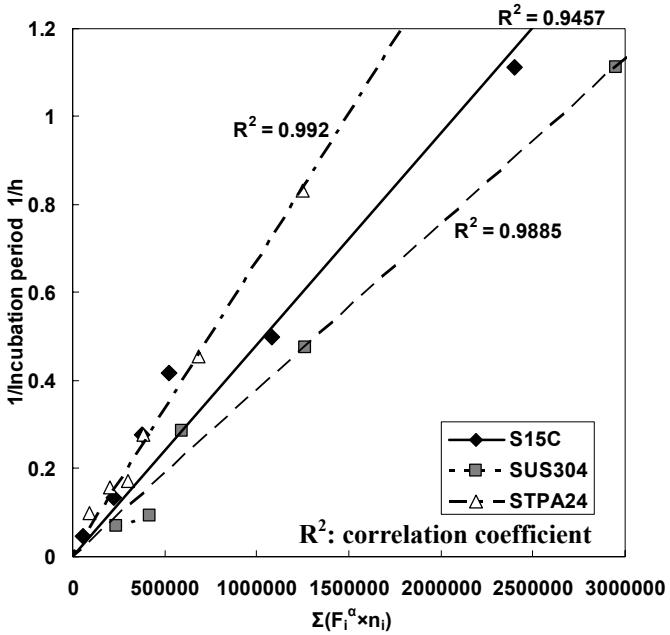

Figure 17: Relation between $\sum(F_i^{\alpha}\times n_i)$ and reciprocal of the incubation period

CONCLUSIONS

In this study, we proposed a prediction method for the incubation period with the cavitating liquid jet method which is based on two sets of erosion tests and on measurements of bubble collapse impact loads. We clarified the following points.

(1) Since the relation between the parameter $\sum(F_i^{\alpha}\times n_i)$ and the reciprocal of the incubation period shows a proportional relation, the parameter $\sum(F_i^{\alpha}\times n_i)$ is suitable for the evaluation of cavitation erosion.

(2) After the constants α and C have been obtained under two different cavitation conditions, we can predict the incubation period with the cavitating liquid jet method under yet another condition, provided that the bubble collapse impact loads are measured.

NOMENCLATURE

c: sound velocity in the test liquid
C: constant depending on the material
e: impact energy
e_1: rebound restitution coefficient
E: cumulative impact energy
F: impact load obtained from steel ball drop test
F_i: bubble collapse impact load
g: acceleration of gravity
h_0: height in which the steel ball is dropped
m: mass of the steel ball
n_i: number of impacts
N_i: number of cycles to fracture, number of impacts at the termination of the incubation period with constant impact load F_i
p_d: downstream pressure
p_u: upstream pressure
p_v: vapor pressure
t_d: incubation period (subscript d indicates the flow velocity)

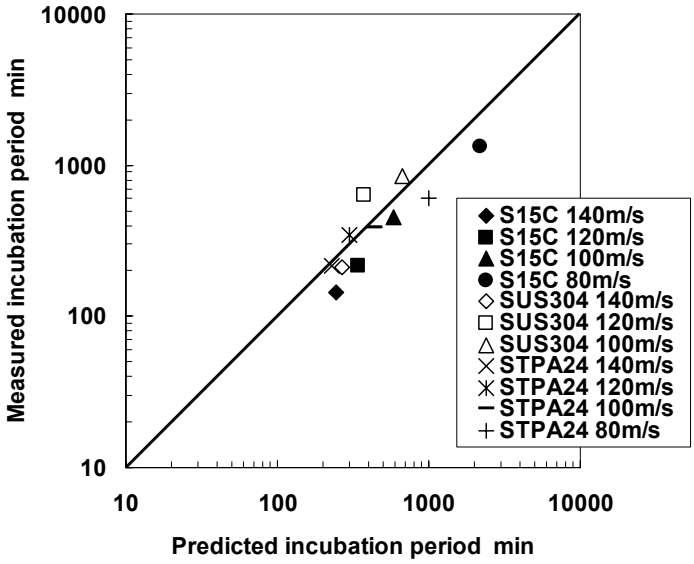

Figure 18: Prediction accuracy for each flow velocity

V: flow velocity
V_0: impact velocity at a steel ball drop test
V_{in}: input voltage of the measuring system for the calibration coefficient of the circuit
V_{out}: output voltage of the measuring system for the calibration coefficient of the circuit
α: constant depending on the material
ρ: liquid density
σ: cavitation number
σ_i: rotary bending stress
ΔT: hold time of the impact load
ΔV: maximum voltage obtained from a steel ball drop test
$\sum F_i^2$: equivalent value to impact energy

REFERENCES

[1] Hattori, S., Mori, H. and Okada, T. 1998, Trans. ASME, Journal of Fluids Engineering, Vol. 120, 179-185.
[2] Iwai, Y., Tanaka, S. and Okada, T. 1988, Transactions of the Japan Society of Mechanical Engineers, Series A, Vol. 54, No. 500, 861-867.
[3] Soyama, H., Ono, S. and Harada, I. 2007, The 9th AICFM, Jeju, Korea, No. AICFM 9-037.
[4] Hattori, S., Kishimoto, M. and Sugiyama, K. 2008, Proceedings of JSME annual meeting, No. 087-1, 3-4. (in Japanese)
[5] ASTM Designation 2005, G134-95, Annual Book of ASTM Standards, 561-572.
[6] Hattori, S., Maekawa, N. and Kuwabara, M. 2001-3, Transactions of the Japan Society of Mechanical Engineers, Series A, Vol. 67, No. 655, 470-475.
[7] Hattori, S., Ishikura, R. and Zhang, Q. 2004, Wear, 257, 1022-1029.
[8] De, M. K. and Hammitt, F. G. 1982, Trans. ASTM, Journal of Fluids Engineering, 104, 434-442.
[9] Hattori, S., Sun, B. and Hammitt, F. G. 1985, Wear, 103, 119-131.
[10] Hammitt, F. G. 1980, "Cavitation and multiphase flow phenomena", McGraw-Hill Inc., 229.
[11] Vaidya, S. and Preece, C. M. 1978, Metal Trans. Series A, 9A, 229.
[12] de Jonge, J. B. and Nederveen, A. 1980, ASTM STP 714, 170-184.
[13] Nakamura, H. 1981, JSMS, Committee Meeting on Fatigue Research, No. 158.